Nanoscale Advances

PAPER

View Article Online
View Journal | View Issue

Cite this: *Nanoscale Adv.*, 2019, **1**, 827

Effect of chloride substitution on interfacial charge transfer processes in $MAPbI_3$ perovskite thin film solar cells: planar *versus* mesoporous†

Zhongguo Li, [ab] Charles Kolodziej, [a] Christopher McCleese, [a] Lili Wang, [a] Anton Kovalsky, [a] Anna Cristina Samia, [a] Yixin Zhao [c] and Clemens Burda *[a]

For photovoltaic devices based on hybrid organic–inorganic perovskite thin films, the cell architecture is a vital parameter in defining the macroscopic performance. However, the understanding of the correlation between architecture and carrier dynamics in perovskite thin films has remained elusive. In this work, we utilize concerted materials characterization and optical measurements to investigate the role of chloride addition in PSC devices with two different architectures. Perovskite thin films, prepared with varying ratios of methylammonium halide MACl : MAI (0 : 1, 0.5 : 1, 1 : 1, and 2 : 1), were coated on either planar or mesoporous TiO_2/FTO substrates. X-ray diffraction analysis reveals that with increasing the ratio of the Cl^- precursor, there is an increasing preferential directional growth of the perovskite film in both configurations. Time-resolved photoluminescence spectroscopy was applied to investigate the electron injection dynamics from the photoexcited perovskites to the TiO_2. It is found that the interfacial electron injection rate from perovskite to planar TiO_2 is accelerated with increasing Cl^- content, which explains the increased power conversion efficiencies using Cl^--modified perovskites as photoactive materials. In contrast, Cl^- addition demonstrate no discernable influence on electron injection to mesoporous TiO_2, suggesting the interfacial charge recombination rather than electron injection give rise to the improved performance observed in the mesoporous configuration. The results presented here, provide a deeper understanding of the mechanism of chloride addition to $MAPbI_3$ solar cells with different architectures.

Received 30th October 2018
Accepted 15th November 2018

DOI: 10.1039/c8na00317c

rsc.li/nanoscale-advances

Introduction

Over the last decade, hybrid organic–inorganic perovskite solar cells (PSC) have attracted tremendous research interest owing to their fascinating properties such as high power conversion efficiencies (PCE), low fabrication cost, ease of preparation, *etc.* To date, the highest device efficiency of PCS has reached over 23%, indicating their outstanding potential for future commercialization.[1,2] Considerable research efforts have been devoted to optimizing the efficiencies of PSCs by varying the architecture,[3] deposition methods,[4] precursor compositions,[5–7] partial substitution of the A, B, and/or X-sites[8,9] and the charge carrier extraction materials,[10–12] to name a few. However, the fundamental photo-physical mechanism of working PSC devices, in particular the charge carrier separation, transport and recombination, is still a point of contention at present. Consequently, it is of great importance to clarify the carrier separation and recombination dynamics within PSCs for increasing their light-to-energy conversion efficiency.

One promising approach to increase the PCE is the addition of chloride, in the form of $PbCl_2$ or CH_3NH_3Cl (MACl), to the perovskite precursor solution.[13,14] With chloride substitution, mixed perovskites have shown extended charge carrier diffusion lengths, surface passivation, and improved crystallinity.[15,16] However, there are contending viewpoints in the literature on the role of chloride substitution in PSC thin films. In earlier work, it was reported that although a chloride source was added in the original precursor solution, no chloride was detected in the final annealed film.[17,18] Using more sensitive techniques such as X-ray photoelectron spectroscopy (XPS) and photo-thermally induced resonance, there have been multiple reports about the presence of chloride within such perovskite films.[19–22] Despite this extensive work, it is not clear as to whether these chloride ions are substituting for iodide, are interstitially added, or if they accumulate at grain boundaries. One hypothesis has been that Cl^- is situated at the interface between the

[a]*Department of Chemistry, Case Western Reserve University, 10900 Euclid Ave., Cleveland, OH 44106, USA. E-mail: burda@case.edu*

[b]*College of Physics and Electronic Engineering, Changshu Institute of Technology, No. 99 3rd South Ring Road, Changshu 215500, China*

[c]*School of Environmental Science and Engineering, Shanghai Jiao Tong University, 800 Dongchuan Rd., Shanghai 200240, China*

† Electronic supplementary information (ESI) available: Experimental details of sample preparation, detailed assignment of XRD patterns, instrument response function for the time-resolved PL measurements, TRPL contour plot and kinetic trace of $MAPbI_3$ single crystal. See DOI: 10.1039/c8na00317c

perovskite and the TiO_2 electron acceptor layer, which is known to be an effective route to improve the electron injection efficiencies.[23–26] It has also been theoretically shown that the presence of Cl^- diminishes inelastic electron–phonon coupling between the lowest energy electron and hole states which helps to reduce nonradiative losses.[27] Chen *et al.* reported that the charge injection rate is higher when a mixed-halide perovskite is coated on PCBM in the planar architecture compared to the rate using pristine perovskite.[28] However, for mesoporous PSC devices, a clear understanding of the impact of Cl addition on the charge carrier separation dynamics remains elusive, thus far.

It is well-established that the architecture of PSCs plays a decisive role in determining the performance of the perovskite device. Structural differences lead to changes in both the electronic and optical properties of the perovskites and in turn affect device performance. It has been shown that the structure can alter optical properties, carrier mobility, and grain size.[29,30] To date, there are a handful of studies about the charge transfer dynamics in PSC devices with planar and mesoscopic morphologies.[31–34] Despite such great efforts, the correlation between architecture and mixed perovskite has largely remained unexplored. Therefore, a clear identification of the role of chloride addition on the optoelectronic properties of PSCs with different architectures needs to be explored.

In this work, we synthesized mixed $MAPbI_3$ thin films with varying chloride additions and characterized their structural and optical properties to better understand how the Cl^-/I^- ratio affects the interfacial charge carrier dynamics in PSC devices. The novelty of this work is that we have characterized the kinetics of carrier injection in mixed $MAPbI_3$ solar cells with both planar and mesoporous architectures. We compare different mixed-halide $MAPbI_{3-x}Cl_x$ solar cells fabricated under identical conditions that differ only in the ETL layer, therefore decouple the composition impact from device performance. The presented results clearly demonstrate that Cl^- addition leads to improvement of cell efficiencies. However, the mechanism behind these improvements is dramatically different in planar and mesoscopic architectures. In the following we detail related results and discuss the observed differences. This understanding could be useful for the development of future mixed-halide perovskite optoelectronic devices.

Experimental results

All reagents were purchased from Sigma Aldrich and used as received without further purification. Four samples with MACl : MAI = 0 : 1 (0 MACl), 0.5 : 1 (0.5 MACl), 1 : 1 (1 MACl), and 2 : 1 (2 MACl) were synthesized and deposited on planar or mesoporous TiO_2 coated FTO substrates using the method described by Zhao *et al.* earlier.[14] The detailed experimental procedures are included in the ESI.† These architectures are illustrated in Scheme 1.

X-ray diffraction (XRD) measurements were performed to characterize the crystal structure of the perovskite films and the diffraction patterns are shown in Fig. 1. To determine the average grain size of each sample Rietveld analysis was performed and the results are reported in Table 1. It is found that for the planar architecture, as the MACl : MAI precursor ratio increased from 0 MACl to 2 MACl, the grain size of the resulting perovskite film increases from 28 to 46 nm, respectively. This is not the case for the mesoporous architectures. The 0 MACl and 2 MACl samples show the largest grain size of 36 nm and the 0.5 MACl and 1 MACl have grain sizes of 22 and 27 nm, respectively. Enhanced views and complete indexing of the peaks for the 0 MACl and 0.5 MACl perovskites on both architectures are shown in Fig. S1.† Both planar samples show a pure perovskite structure with some FTO peaks from the substrate. The 0 MACl mesoporous sample shows peaks for perovskite, PbI_2 ($2\Theta = 12.7°$), and TiO_2 ($2\Theta = 25.5°$). By adding 0.5 MACl, the PbI_2 peak disappears and a pure perovskite pattern is observed.

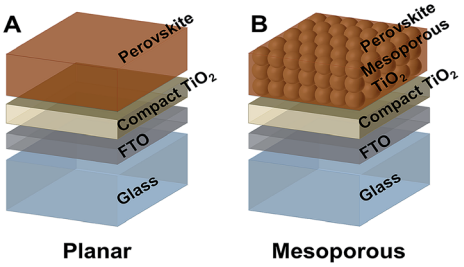

Scheme 1 Illustration of the sample architectures studied in this work. (A) "Planar" architecture consisting of perovskite/planar TiO_2/FTO and (B) the "mesoporous" architecture consisting of perovskite/mesoporous TiO_2/planar TiO_2/FTO.

Based on the Rietveld analysis, additional MACl in the planar architectures facilitates the growth of larger perovskite grains, but not so in mesoporous architectures. It has been reported that an increase in the grain size leads to an increase in the charge carrier diffusion length, which can be as large as hundreds of microns to millimeters for perovskite single crystals.[35] Grain boundaries could act as nonradiative recombination centers, which can be detrimental to device efficiencies.[15] Therefore by growing larger grains with increasing additions of MACl, the number of grain boundaries is reduced and this could be one reason for the large increase in PCE in planar devices, see Table 1. However, in mesoporous samples, the addition of MACl leads to mainly smaller grains. Although the grain size for these mesoporous samples decreased, device efficiencies marginally increased with increasing the ratio of MACl. Therefore, it is now evident that the increase in grain size is not the only contributing factor for the increase in device efficiency.

In Fig. 1, we find a relative increase of the (110) and (220) diffraction peak intensities with increasing MACl. Since no other peaks increase significantly in intensity with the addition of MACl, we attribute the relative increase of the (110) and (220) peaks to preferential growth of these lattice plains. By comparing XRD intensities between the two architectures, we find that the ratio of the (110) to (200) peak for the planar samples is larger (13 : 1) than that of the peak intensity ratio of the mesoporous sample (5.6 : 1). This indicates that the

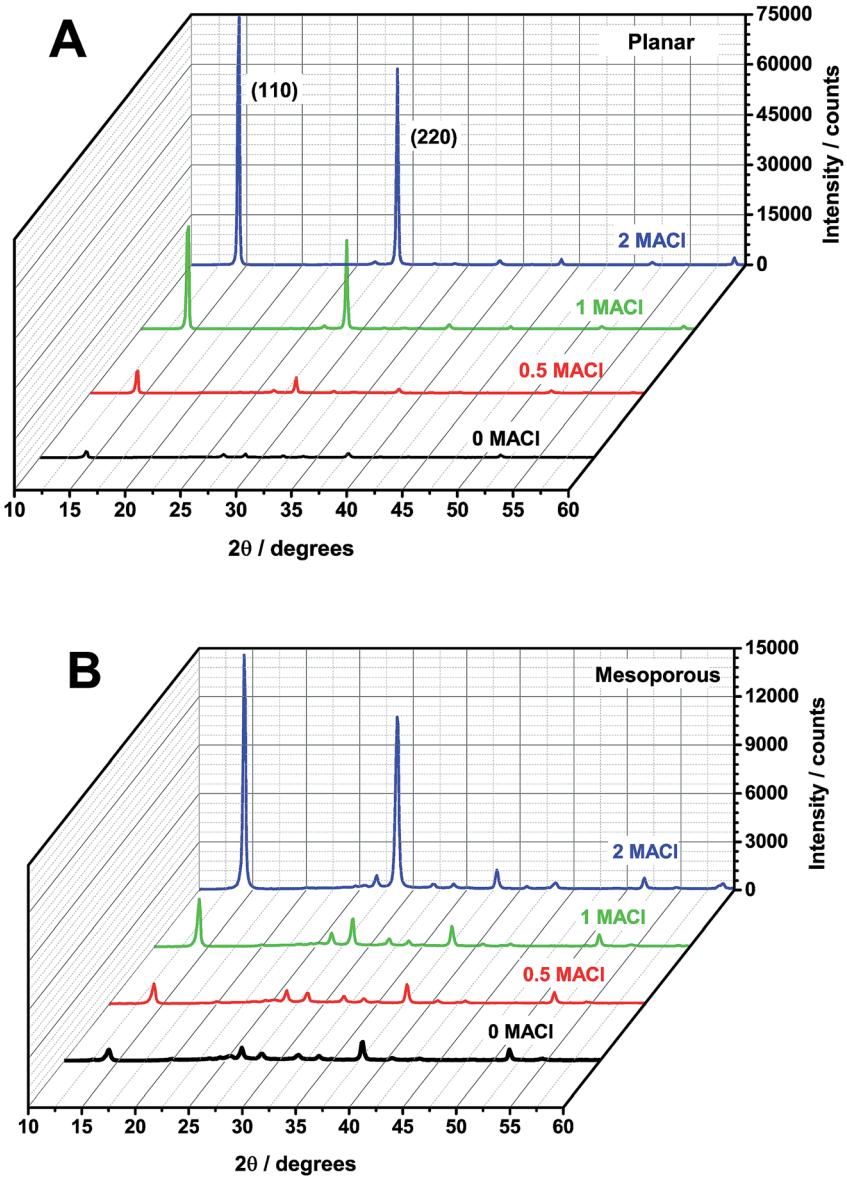

Fig. 1 XRD of the perovskite films with 0 MACl (black), 0.5 MACl (red), 1 MACl (green), and 2 MACl (blue) precursor ratios coated on (A) planar and (B) mesoporous titania. The (110) and (220) peaks are labeled here and all peaks are further indexed in Fig. S1.†

Table 1 Grain size, PL wavelength (λ_{PL}), PL FWHM, PL decay lifetimes (τ_{PL}), PL rate constants (k_{PL}), injection rate constants (k_{inj}), injection efficiencies (ϕ_{inj}), and PCEs (η) of perovskite films on planar or mesoporous TiO_2 coated FTO substrates

Architecture	Sample	Grain size (nm)	λ_{PL} (nm)	FWHM (nm)	τ_{PL} (±0.19 ns)	k_{PL} (s^{-1})	k_{inj} (s^{-1})	ϕ_{inj} (%)	η_f[a] (%)
Planar	0 MACl	28	775	52	2.68	3.7×10^8	2.1×10^8	52	1.34
	0.5 MACl	39	778	49	2.27	4.4×10^8	2.7×10^8	59	9.50
	1 MACl	42	786	41	1.77	5.6×10^8	4.0×10^8	68	10.51
	2 MACl	46	784	47	0.98	1.0×10^9	8.5×10^8	83	10.85
Mesoporous	0 MACl	36	765	41	1.40	7.1×10^8	5.5×10^8	75	7.64
	0.5 MACl	22	754	54	1.05	9.5×10^8	7.9×10^8	81	9.12
	1 MACl	27	757	54	1.07	9.3×10^8	7.7×10^8	81	9.57
	2 MACl	36	766	57	1.18	8.5×10^8	6.8×10^8	79	10.09

[a] From ref. 14.

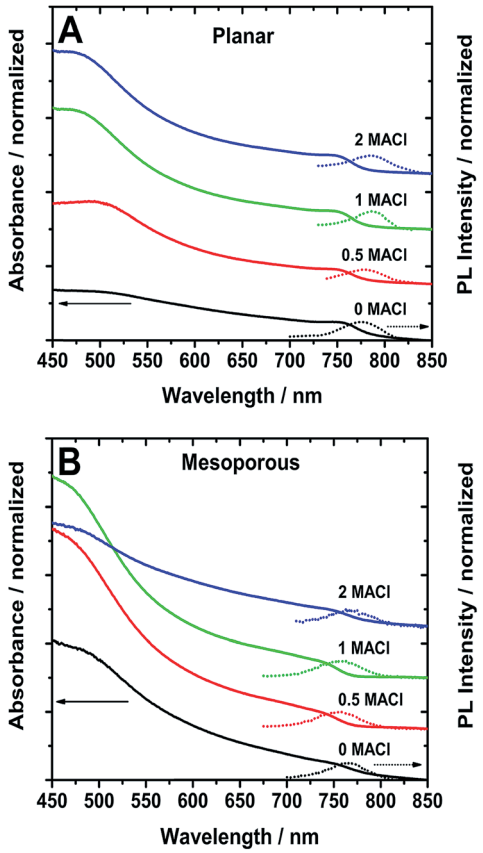

Fig. 2 Ground state UV-visible absorption (solid) and steady state PL (dotted) spectra of 0 MACl (black), 0.5 MACl (red), 1 MACl (green), and 2 MACl (blue) in (A) planar and (B) mesoporous architecture.

preferential growth of the (110) plane is greater for planar samples, which agrees well with the pervious report.[36] This tendency may further explain why there is such a dramatically improved increase in the PCE with increasing addition of MACl for planar devices, compared to the mesoporous samples.[14]

The absorption spectra in Fig. 2 show that the planar samples have a defined band edge peak while the absorption onset of the mesoporous ones appear as a broad shoulder. The measured PL maxima are reported in Table 1. In the planar samples, the PL maximum red-shifts from 775 to 784 nm as the ratio of MACl increases. On the other hand, the mesoporous samples show similar PL wavelengths of ~765 nm for the 0 MACl and 2 MACl samples, which are longer than the 0.5 MACl and 1 MACl PL wavelengths at 754 and 757 nm, respectively. Like the absorption, the emission of planar perovskite films is narrower (FWHM) compared to the mesoporous ones (Table 1). These narrower PL and absorption features indicate that the planar samples exhibit a more uniform film composition compared to the mesoporous samples.

Time-resolved photoluminescence measurements (TRPL) were performed to study the effect of the addition of MACl in the precursor solution and the support architecture on the optical properties of the perovskite films. TRPL spectra of perovskite with planar (A–D) and mesoporous (E–H) architectures are shown in Fig. 3. TRPL decay kinetics were obtained by measuring the relaxation dynamics at the wavelength of greatest PL intensity and are shown in Fig. 4 and the lifetimes obtained from fitting the curves with a single exponential decay equation have been summarized in Table 1. It is found that the radiative carrier lifetimes of the planar architectures decreased as the chloride content increased. On the other hand, the mesoporous samples showed no obvious trend between the

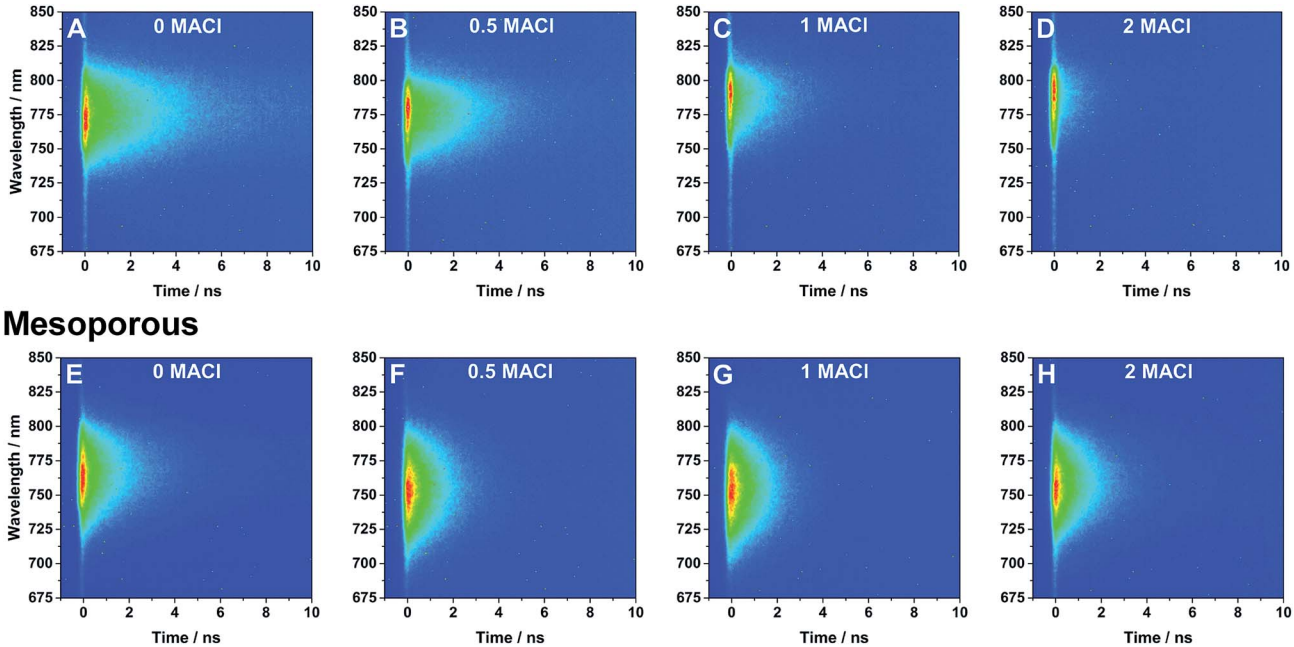

Fig. 3 TRPL spectra of perovskite films with various ratios of MACl precursor (noted in figure) on (A–D) planar and (E–H) mesoporous TiO_2 excited using 480 nm light.

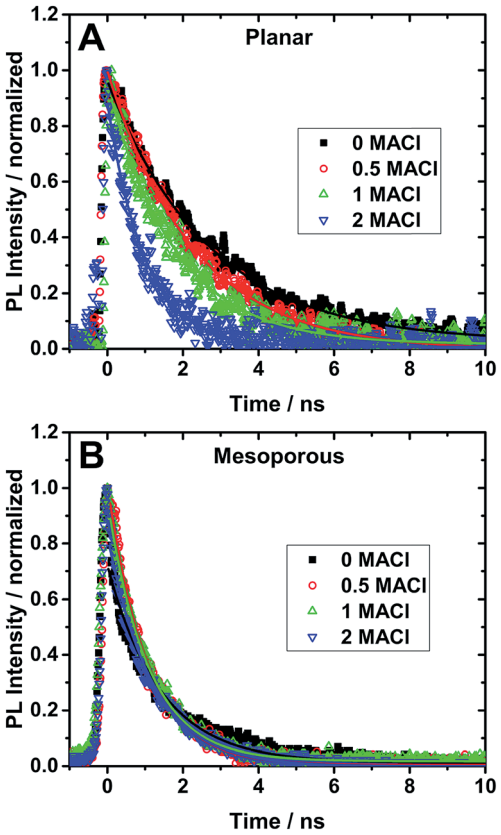

Fig. 4 TRPL decay dynamics (symbols) and their fits (lines) of perovskite films on (A) planar TiO_2 and (B) mesoporous TiO_2 coated FTO substrates excited using 480 nm light. The lifetimes obtained from the single exponential fits are reported in Table 1.

samples other than that all samples with MACl showed a slightly faster decay compared to the sample without MACl.

Recent studies have shown that the presence of PbI_2 in perovskite films can affect the charge carrier dynamics.[31,37] Looking at the XRD patterns in Fig. 1, there is no PbI_2 present in any of the films prepared using MACl and therefore all observed kinetics are assumed to be largely due to the intrinsic properties of the perovskite/titania/FTO interfaces. The planar architectures studied in this work show a PL lifetime of 2.68 ns for 0 MACl and this lifetime is progressively shortened to 0.98 ns for 0.5, 1, and 2 equivalents of MACl. This decrease in PL lifetime together with the measured increase in PCE indicates that in the planar structure charge carrier injection is accelerated with Cl^- addition, which agrees well with pervious report.[28] On the other hand, the decay dynamics for the mesoporous architectures shows a lifetime of 1.4 ns for the 0 MACl perovskite sample. Upon the addition of chloride, it is found that the PL lifetime is shortened to 1.05 ns (0.5 MACl) at best. These results demonstrate that Cl addition has a much weaker, if not different, impact on the charge carrier dynamics in mesoporous structures.

Freestanding $MAPbI_3$ single crystals were synthesized to compare how the injection lifetimes of these films differ from the intrinsic perovskite PL lifetime in the absence of a charge collection layer. These single crystals were characterized using both SEM and XRD (Fig. S3†). The TRPL contour plot and the decay kinetics for the single crystal measurements are shown in Fig. S4.† The average PL decay lifetime of single crystal can be estimated to 5.6 ns using the procedure in previous report.[38] Using the 5.6 ns PL lifetime from the single crystal as an unquenched reference, the charge carrier injection efficiency (ϕ_{inj}) can be calculated using eqn (1). Here the injection rate constant (k_{inj}) is defined as $k_{inj} = k_{film} - k_{SC}$, where k_{film} and k_{SC} is the PL rate constant determined from the PL lifetimes of the perovskite films and single crystal, respectively.[39]

$$\phi_{inj} = k_{inj}/(k_{inj} + k_{SC}) \quad (1)$$

For the planar sample, the injection efficiency increases from 52% (for the 0 MACl sample) to 83% (for the 2 MACl sample). There is only a small enhancement of ϕ_{inj} for the mesoporous samples from 75% to 81%. This result further demonstrates that the addition of chloride leads to significant enhanced charge carrier injection into the planar TiO_2 structure but has negligible impact in the mesoporous TiO_2 structures.

Discussion

Based on the results above, we attempt to identify the link between the role of chloride addition, perovskite morphology and the device performance. The key points learnt from the measurements above are as follows: (i) chloride addition leads to larger grain size in the planar architecture, while it has no significant effect on grain size in the mesoporous architecture. (ii) Chloride addition is beneficial to the growing of (110)-oriented perovskite films on both planar and mesoporous architectures, but the effect is more pronounced in the planar structure. (iii) Electron injection rates from the perovskite layers into planar TiO_2 layers become significantly faster with chloride addition, but electron injection rates into the mesoporous TiO_2 scaffold have only a weak dependence on chloride addition to the perovskite. In the discussion below, we consider the impact of chloride addition to perovskite on the charge dynamics in planar and mesoporous architectures.

In the planar architecture, chloride addition not only increases the grain size but also leads to a (110)-oriented perovskite film. It is known that larger grain size is beneficial to the carrier lifetimes and mobilities.[35] Recent theoretical reports also found that the (110) face is the one that leads to the best interaction between the perovskite and the TiO_2 electron acceptor layer.[25] Furthermore, we have recently shown that the electron diffusion length along the (110) crystallographic plane is on the order of 10 μm which further demonstrates the benefits of the addition of MACl.[16] On the other hand, pervious literature showed that interfacial electron transfer from pristine $MAPbI_3$ to planar TiO_2 is rather slow (>100 ns), which may relate to the limited surface area of the planar TiO_2 and small Gibbs free energy difference between the perovskite and TiO_2 conduction band edges.[33,34] The TRPL results above show that interfacial charge injection rate is enhanced by chloride addition in the planar architecture, plausibly owing to the better interfacial contact between the perovskite and TiO_2. Therefore,

the improvement of grain size and interfacial coupling in planar perovskites explain the nearly 30% increase in ϕ_{inj} with the addition of MACl.

In the mesoporous architecture, the grain size and interfacial charge injection rate are independent of chloride addition. The former is likely due to the pore filling of mesoporous TiO_2 scaffold.[40] The latter can be explained by the band alignment in perovskite/mesopores TiO_2 heterojunction. Recent depth-resolved XPS measurement show that the perovskite/mesopores TiO_2 has a graded electronic band structure near the interface.[41] Kelvin probe force microscopy (KPFM) measurements suggest that the mesoporous perovskite films had a fixed p–n junction located at the perovskite/mesopores TiO_2 interface regardless of the variation in perovskite composition.[42] Therefore, chloride addition has a different role in PCE enhancement of mesoporous perovskite solar cells. Taking into account all results above, the most plausible role is related to the interfacial charge recombination between TiO_2 and the perovskite layers. Recently, photoinduced transient photovoltage measurements show that there is a slow interfacial charge recombination pathway (on μs time scale) in both planar and mesoporous TiO_2 PSCs. And this component in mesoporous TiO_2 was found to be 20 times slower than that in planar architecture.[43,44] In addition, molecular dynamics stimulation results demonstrate that replacing iodines by chlorines at the perovskite/TiO_2 interface can reduce interfacial electron–hole recombination processes.[45,46] We therefore conclude that chloride addition results in retardation of the interfacial charge recombination in the mesoporous structure, and thus to optimized solar cell performance.

When comparing between the planar and mesoporous structures, it is found that the electron injection rates and efficiencies are greater in mesoporous films than in planar ones, for all chloride levels, except for 2 MACl. This work highlights that not only the electron injection but also carrier recombination need to be taken into account to optimize the performance of photovoltaic devices. Our results suggest that the optimum solar cell configuration for $MAPbI_3$ perovskite, with little or no chloride, is the mesoporous TiO_2 structure. However, ϕ_{inj} for 2 MACl substituted perovskite is greater for the planar architectures, which suggests that the appropriate perovskite solar cell structure for high amounts of Cl^- addition may be the planar one.

Conclusions

In summary, we have investigated the effect of chloride addition on the morphology and interfacial charge transfer dynamics of $MAPbI_3$ perovskite thin films with both planar and mesoporous TiO_2 architectures. The XRD and time-resolved photoluminescence spectroscopy measurements demonstrate that the grain size and interfacial charge injection rates are improved by chloride addition in the planar architecture. This explains the optimized solar cell performance. However, in mesoporous structures, both the grain size and interfacial charge injection rate are found to be independent of chloride addition, suggesting a retarded interfacial charge recombination between perovskite and TiO_2 leads to the measured enhancement in PCE.

Conflicts of interest

All authors declare no competing financial interests.

Acknowledgements

CB acknowledges support from Case Western Reserve University for the Center for Chemical Dynamics and Nanomaterials Research. ZGL acknowledges support from the National Natural Science Foundation of China (grant 11704048) and the China Scholarship Council (No. 201708320116). YZ acknowledges the support of the NSFC (Grant 21777096).

References

1 Y. Rong, Y. Hu, A. Mei, H. Tan, M. I. Saidaminov, S. I. Seok, M. D. McGehee, E. H. Sargent and H. Han, *Science*, 2018, **361**, eaat8235.
2 J. Huang, Y. Yuan, Y. Shao and Y. Yan, *Nat. Rev. Mater.*, 2017, **2**, 17042.
3 H. C. Kwon, W. Yang, D. Lee, J. Ahn, E. Lee, S. Ma, K. Kim, S. C. Yun and J. Moon, *ACS Nano*, 2018, **12**, 4233.
4 D. Luo, W. Yang, Z. Wang, A. Sadhanala, Q. Hu, R. Su, R. Shivanna, G. F. Trindade, J. F. Watts, Z. Xu, T. Liu, K. Chen, F. Ye, P. Wu, L. Zhao, J. Wu, Y. Tu, Y. Zhang, X. Yang, W. Zhang, R. H. Friend, Q. Gong, H. J. Snaith and R. Zhu, *Science*, 2018, **360**, 1442.
5 W. S. Yang, B. W. Park, E. H. Jung, N. J. Jeon, Y. C. Kim, D. U. Lee, S. S. Shin, J. Seo, E. K. Kim, J. H. Noh and S. I. Seok, *Science*, 2017, **356**, 1376.
6 S. Gharibzadeh, F. Valduga de Almeida Camargo, C. Roldan-Carmona, G. C. Gschwend, J. Pascual, R. Tena-Zaera, G. Cerullo, G. Grancini and M. K. Nazeeruddin, *Adv. Mater.*, 2018, 1801496.
7 J. Feng, X. Zhu, Z. Yang, X. Zhang, J. Niu, Z. Wang, S. Zuo, S. Priya, S. Liu and D. Yang, *Adv. Mater.*, 2018, 1801418.
8 M. Abdi-Jalebi, Z. Andaji-Garmaroudi, S. Cacovich, C. Stavrakas, B. Philippe, J. M. Richter, M. Alsari, E. P. Booker, E. M. Hutter, A. J. Pearson, S. Lilliu, T. J. Savenije, H. Rensmo, G. Divitini, C. Ducati, R. H. Friend and S. D. Stranks, *Nature*, 2018, **555**, 497.
9 L. Fan, Y. Ding, J. Luo, B. Shi, X. Yao, C. Wei, D. Zhang, G. Wang, Y. Sheng, Y. Chen, A. Hagfeldt, Y. Zhao and X. Zhang, *J. Mater. Chem. A*, 2017, **5**, 7423.
10 H. Tan, A. Jain, O. Voznyy, X. Lan, F. P. G. de Arquer, J. Z. Fan, R. Quintero-Bermudez, M. Yuan, B. Zhang, Y. Zhao, F. Fan, P. Li, L. N. Quan, Y. Zhao, Z. H. Lu, Z. Yang, S. Hoogland and E. H. Sargent, *Science*, 2017, **355**, 722.
11 F. Biccari, F. Gabelloni, E. Burzi, M. Gurioli, S. Pescetelli, A. Agresti, A. E. D. R. Castillo, A. Ansaldo, E. Kymakis, F. Bonaccorso, A. D. Carlo and A. Vinattieri, *Adv. Energy Mater.*, 2017, **7**, 1701349.

12 C. Ding, Y. Zhang, F. Liu, Y. Kitabatake, S. Hayase, T. Toyoda, K. Yoshino, T. Minemoto, K. Katayama and Q. Shen, *Nano Energy*, 2018, **53**, 17.
13 S. D. Stranks, G. E. Eperon, G. Grancini, C. Menelaou, M. J. P. Alcocer, T. Leijtens, L. M. Herz, A. Petrozza and H. J. Snaith, *Science*, 2013, **342**, 341.
14 Y. Zhao and K. Zhu, *J. Phys. Chem. C*, 2014, **118**, 9412.
15 D. W. deQuilettes, S. M. Vorpahl, S. D. Stranks, H. Nagaoka, G. E. Eperon, M. E. Ziffer, H. J. Snaith and D. S. Ginger, *Science*, 2015, **348**, 683.
16 S. Liu, L. Wang, W. C. Lin, S. Sucharitakul, C. Burda and X. P. A. Gao, *Nano Lett.*, 2016, **16**, 7925.
17 A. Dualeh, N. Tetreault, T. Moehl, P. Gao, M. K. Nazeeruddin and M. Gratzel, *Adv. Funct. Mater.*, 2014, **24**, 3250.
18 M. I. Dar, N. Arora, P. Gao, S. Ahmad, M. Gratzel and M. K. Nazeeruddin, *Nano Lett.*, 2014, **14**, 6991.
19 E. Edri, S. Kirmayer, M. Kulbak, G. Hodes and D. Chen, *J. Phys. Chem. Lett.*, 2014, **5**, 429.
20 H. Yu, F. Wang, F. Xie, W. Li, J. Chen and N. Zhao, *Adv. Funct. Mater.*, 2014, **24**, 7102.
21 J. Chae, Q. Dong, J. Huang and A. Centrone, *Nano Lett.*, 2015, **15**, 8114.
22 V. L. Pool, A. Gold-Parker, M. D. McGehee and M. F. Toney, *Chem. Mater.*, 2015, **27**, 7240.
23 C. W. Chen, H. W. Kang, S. Y. Hsiao, P. F. Yang, K. M. Chiang and H. W. Lin, *Adv. Mater.*, 2014, **26**, 6647.
24 S. Colella, E. Mosconi, G. Pellegrino, A. Alberti, V. L. P. Guerra, S. Masi, A. Listorti, A. Rizzo, G. G. Condorelli, F. De Angelis and G. Gigli, *J. Phys. Chem. Lett.*, 2014, **5**, 3532.
25 E. Mosconi, E. Ronca and F. De Angelis, *J. Phys. Chem. Lett.*, 2014, **5**, 2619.
26 M. Jiang, J. Wu, F. Lan, Q. Tao, D. Gao and G. Li, *J. Mater. Chem. A*, 2015, **3**, 963.
27 J. Liu and O. V. Prezhdo, *J. Phys. Chem. Lett.*, 2015, **6**, 4463.
28 Q. Chen, H. Zhou, Y. Fang, A. Z. Stieg, T. B. Song, H. H. Wang, X. Xu, Y. Liu, S. Lu, J. You, P. Sun, J. McKay, M. S. Goorsky and Y. Yang, *Nat. Commun.*, 2015, **6**, 7269.
29 M. F. M. Noh, C. H. Teh, R. Daik, E. L. Lim, C. C. Yap, M. A. Ibrahim, N. A. Ludin, A. R. bin Mohd Yusoff, J. Jang and M. A. M. Teridi, *J. Mater. Chem. C*, 2018, **6**, 682.
30 T. Leijtens, S. D. Stranks, G. E. Eperon, R. Lindblad, E. M. J. Johansson, I. J. McPherson, H. Rensmo, J. M. Ball, M. M. Lee and H. J. Snaith, *ACS Nano*, 2014, **8**, 7147.
31 L. Wang, C. McCleese, A. Kovalsky, Y. Zhao and C. Burda, *J. Am. Chem. Soc.*, 2014, **136**, 12205.
32 E. M. Hutter, G. E. Eperon, S. D. Stranks and T. J. Savenije, *J. Phys. Chem. Lett.*, 2015, **6**, 3082.
33 A. R. Pascoe, M. Yang, N. Kopidakis, K. Zhu, M. O. Reese, G. Rumbles, M. Fekete, N. W. Duffy and Y. B. Cheng, *Nano Energy*, 2016, **22**, 439.
34 M. Liu, M. Endo, A. Shimazaki, A. Wakamiya and Y. Tachibana, *ACS Appl. Energy Mater.*, 2018, **1**, 3722.
35 Q. Dong, Y. Fang, Y. Shao, P. Mulligan, J. Qiu, L. Cao and J. Huang, *Science*, 2015, **347**, 967.
36 Q. Wang, M. Lyu, M. Zhang, J. H. Yun, H. Chen and L. Wang, *J. Phys. Chem. Lett.*, 2015, **6**, 4379.
37 Q. Chen, H. Zhou, T. B. Song, S. Luo, Z. Hong, H. S. Duan, L. Dou, Y. Liu and Y. Yang, *Nano Lett.*, 2014, **14**, 4158.
38 D. Yang, R. Yang, J. Zhang, Z. Yang, S. Liu and C. Li, *Energy Environ. Sci.*, 2015, **8**, 3208.
39 K. C. Lin, L. Wang, T. Doane, A. Kovalsky, S. Pejic and C. Burda, *J. Phys. Chem. B*, 2014, **118**, 14027.
40 T. Leijtens, B. Lauber, G. E. Eperon, S. D. Stranks and H. J. Snaith, *J. Phys. Chem. Lett.*, 2014, **5**, 1096.
41 K. Eom, U. Kwon, S. S. Kalanur, H. J. Park and H. Seo, *J. Mater. Chem. A*, 2017, **5**, 2563.
42 M. Cai, N. Ishida, X. Li, X. Yang, T. Noda, Y. Wu, F. Xie, H. Naito, D. Fujita and L. Han, *Joule*, 2018, **2**, 296.
43 N. F. Montcada, J. M. Marin-Beloqui, W. Cambarau, J. Jimenez-Lopez, L. Cabau, K. T. Cho, M. K. Nazeeruddin and E. Palomares, *ACS Energy Lett.*, 2016, **2**, 182.
44 Y. Wang, H. Y. Wang, J. Han, M. Yu, M. Y. Hao, Y. Qin, L. M. Fu, J. P. Zhang and X. C. Ai, *Energy Technol.*, 2017, **5**, 442.
45 R. Long and O. V. Prezhdo, *ACS Nano*, 2015, **9**, 11143.
46 R. Long, J. Liu and O. V. Prezhdo, *J. Am. Chem. Soc.*, 2016, **138**, 3884.